Local stability analysis of azimuthal magnetorotational instability of ideal MHD flows

Zou, Rong
Graduate School of Mathematics, Kyushu University

Fukumoto, Yasuhide
Institute of Mathematics for Industry, Kyushu University

出版情報：Progress of Theoretical and Experimental Physics. 2014 (11), 2014-11-05. 日本物理学会
バージョン：
権利関係：

MI Preprint Series

Mathematics for Industry
Kyushu University

Local stability analysis of azimuthal magnetorotational instability of ideal MHD flows

Rong Zou &
Yasuhide Fukumoto

MI 2014-8

(Received June 5, 2014)

Institute of Mathematics for Industry
Graduate School of Mathematics
Kyushu University
Fukuoka, JAPAN

PTEP

Prog. Theor. Exp. Phys. **2013**, 00000 (17 pages)
DOI: 10.1093/ptep/0000000000

Local stability analysis of azimuthal magnetorotational instability of ideal MHD flows

Rong Zou[1], and Yasuhide Fukumoto[2]

[1] *Graduate School of Mathematics, Kyushu University, Fukuoka, 819-0395, Japan*
[2] *Institute of Mathematics for Industry, Kyushu University, Fukuoka, 819-0395, Japan*
[*] *E-mail: zou@math.kyushu-u.ac.jp, yasuhide@imi.kyushu-u.ac.jp*

Short-wavelength stability analysis is made of axisymmetric rotating flows of a perfectly conducting fluid, subjected to external azimuthal magnetic field B_θ to non-axisymmetric as well as axisymmetric perturbations. When the magnetic field is sufficiently weak, the instability occurs for $Ro = r\Omega'/(2\Omega) < Ro_c$ with Ro_c close to zero and the maximum growth rate close to the Oort A-value $|Ro|$, where $\Omega(r)$ is the angular velocity of the rotating flow as a function only of r, the distance from the axis of symmetry, and the prime designates the derivative in r. As the magnetic field is increased, the flow becomes unstable to waves of very short axial wavelengths for the whole range of Ro when $Rb = r^2(B_\theta/r)'/(2B_\theta) > -3/4$, and to waves of very long axial wavelengths for a finite range of $|Ro|$ when $Rb < -1/2$. For the both waves, the maximum growth rate increases, beyond the Oort A-value, without bound in proportion to $|B_\theta|$.

Subject Index J11, J13, J18, J21, J22

1. Introduction

Since rediscovery of Velikhov and Chandrasekhar's result [1, 2] by Balbus and Hawley [3], the magnetorotational instability (MRI) has attracted great attention as a plausible mechanism for triggering turbulence in the flow of an accretion disk, for promoting outward transport of angular momentum, while the matter accretes the center. There is a well known Rayleigh's criterion for stability of a rotating flow of circular streamlines [4]. Given the angular velocity $\Omega(r)$ as a function only of the distance r from the rotation axis, define the local Rossby number by $Ro = \frac{1}{2}\mathrm{d}\log\Omega/\mathrm{d}\log r = r\Omega'/(2\Omega)$ [5, 6]. Here the prime designates the derivative with respect to r. In terms of the epicyclic frequency $\kappa^2 = (\Omega^2 r^4)'/r^3$, it is expressed as $Ro = \kappa^2/(4\Omega^2) - 1$. If $\kappa^2 \geq 0$ or $Ro \geq -1$ everywhere, such a rotating flow is linearly stable against axisymmetric disturbances [4, 6]. For an accretion disk, the angular velocity could satisfy the Keplerian law: $\Omega(r)^2 r = -\nabla\Phi;\ \Phi = 1/r$, for which $Ro = -3/4$. Rayleigh's criterion may suggest that Keplerian rotation $\Omega \propto r^{-3/2}$ is hydrodynamically stable.

The magnetic field parallel to the rotation axis drastically alters the stability characteristics. If the axial magnetic field is applied, however weak it is, a rotating flow suffers from instability if $Ro < 0$ [1, 2], implying that an accretion disk with Keplerian flow is unstable. We refer this instability to the standard magnetorotational instability (SMRI). The maximum growth rate at a local portion was found to be $3|\Omega|/4$ for a Keplerian rotation [7]. For a general rotating flow of differential rotation $\Omega(r)$ satisfying $Ro < 0$, the most unstable local

instability mode of the SMRI is the axisymmetric one, with the maximum growth rate being $\nu_A = \frac{1}{2}|\mathrm{d}\log\Omega/\mathrm{d}\log r|$, the Oort A-value [7]. A distinguishing feature is that this growth rate is independent of the applied field strength.

When the magnetic field is frozen into the fluid, the differential rotation of the flow generates the azimuthal component of the magnetic field once the magnetic field acquires the radial component which is possibly created by perturbing the axial field [8, 9]. Hence, it is worthwhile to look into the stability of a rotating flow applied by the azimuthal magnetic field and by a combination of the azimuthal and the axial magnetic field. The instability of the former case is called the azimuthal MRI or the AMRI, and the latter is called the helical MRI or the HMRI [5]. The HMRI has been extensively studied for a fluid of very low conductivity, called the inductionless limit [5, 10], because this is relevant to the experimental setting of using a liquid metal of very low conductivity [11]. Recently, an elaborate analysis has also been made for the AMRI in the regime of very low conductivity [12].

For the perfectly conducting case, the AMRI and the HMRI to three-dimensional disturbances of short wavelength were both examined numerically by Balbus and Hawley [8]. They showed occurrence of the instability by conducting numerical computation of linearized equations made simplified by leaving out, by a physical intuition, terms which appeared to be less important when the spatial variation of the basic magnetic field is slow. But they did not give the values of the growth rate or the parameter region for instability. Moreover, we point out that the traditional treatment of the short-wave stability analysis is liable to miss some terms if a WKB-form of the solution is substituted at an early stage. A careful approach to escape from such a pitfall is first to deduce a differential equation for a single component of the displacement field, and thereafter to substitute the WKB form of the solution into the resulting equation. For a circular symmetric flow, the equation for the radial displacement field is known as the Hain-Lüst equation [13, 14]. In this paper, we resort to the Hain-Lüst equation, as augmented with the terms of the basic flow, in its full form, for the AMRI to non-axisymmetric as well as axisymmetric disturbances. The formulation will be made in §2. Section 3 shows that this approach restores the known results of the axisymmetric SMRI and the axisymmetric AMRI.

We shall show in §4 that, when the steady imposed azimuthal magnetic field $B_\theta(r)$ is sufficiently weak, the flow of the Rossby number $Ro = r\Omega'/(2\Omega) < R_c$ is unstable, with the maximum growth rate close to the Oort A-value. The critical Rossby number is close to zero $R_c \approx 0$ depending on $B_\theta(r)$ and the magnetic Rossby number $Rb = r^2(B_\theta/r)'/(2B_\theta)$, in an analogous way as the SMRI. But the situation is totally changed as $B_\theta(r)$ is increased as detailed in §5. For $Rb > -3/4$, the wave of $k \to \infty$ is excited and is likely to become dominant for $Rb > -1/\sqrt{8}$, and, for $Rb < -1/4$, the wave of $k = 0$ is excited and is likely to become dominant for $Rb < -1/\sqrt{8}$. In either case, the lowest azimuthal wavenumbers $m = 0$ and $m = 1$ is the fastest growing mode. The instability mode of $k = 0$ is admitted in a limited range in Ro around $Ro = 0$, whereas the instability mode of $k \to \infty$ is admitted for the whole values of Ro, implying a remarkable fact that there is no critical value of Ro. Moreover, we shall establish that the maximum growth rate is proportional to $|B_\theta|$ and can exceed the Oort A-value. The last section (§6) is devoted to a summary and conclusions.

2. Short-wavelength stability analysis

We consider a circular symmetric flow of an incompressible inviscid fluid with infinite electric conductivity, and the linear stability of a localized disturbance along one of the streamlines, when the steady azimuthal magnetic field $B_\theta(r) = r\mu(r)$ is applied. We assume that the radial wavelength is much small compared with the radius r of the streamline, being a sort of the WKB approximation. We introduce global cylindrical coordinates (r, θ, z) with the z-axis lying on the symmetric axis. The basic state is a rotating flow in equilibrium, with the angular velocity $\Omega(r)$, subject to a steady external magnetic field having the azimuthal and the axial components $r\mu(r)$ and $B_z(r)$.

$$\boldsymbol{U} = r\Omega(r)\boldsymbol{e}_\theta,\ \boldsymbol{B} = r\mu(r)\boldsymbol{e}_\theta + B_z\boldsymbol{e}_z, \tag{1}$$

where $\boldsymbol{e}_\theta$ is the unit vector in the azimuthal direction. After the second half of §3, we focus on the azimuthal field.

The linearized equations of the momentum and the induction equations for disturbance $\tilde{\boldsymbol{u}}$, $\tilde{\boldsymbol{B}}$ and $\tilde{p}$ are

$$\frac{\partial\tilde{\boldsymbol{u}}}{\partial t} + (\tilde{\boldsymbol{u}}\cdot\nabla)\boldsymbol{U} + (\boldsymbol{U}\cdot\nabla)\tilde{\boldsymbol{u}} = -\frac{1}{\rho}(\nabla\tilde{p}) + \frac{1}{\rho\mu_0}(\tilde{\boldsymbol{B}}\cdot\nabla)\boldsymbol{B} + \frac{1}{\rho\mu_0}(\boldsymbol{B}\cdot\nabla)\tilde{\boldsymbol{B}}, \tag{2}$$

$$\frac{\partial\tilde{\boldsymbol{B}}}{\partial t} = \nabla\times(\boldsymbol{u}\times\tilde{\boldsymbol{B}}) + \nabla\times(\tilde{\boldsymbol{u}}\times\boldsymbol{B}), \tag{3}$$

$$\nabla\cdot\tilde{\boldsymbol{u}} = 0, \tag{4}$$

$$\nabla\cdot\tilde{\boldsymbol{B}} = 0, \tag{5}$$

where the density ρ is assumed to be constant, and the last equation is the solenoidal property of the magnetic field. The first step is to assume the disturbances $\tilde{\boldsymbol{u}}$, $\tilde{\boldsymbol{B}}$ and $\tilde{p}$ in the normal-mode form $\exp[\lambda t + i(m\theta + kz)]$. Then the linearized equations (2)–(5) combine into matrix form for $\boldsymbol{\xi} = (\tilde{u_r},\ \tilde{u_\theta},\ \tilde{u_z},\ \tilde{B_r},\ \tilde{B_\theta},\ \tilde{B_z},\ \tilde{p})$ as

$$\mathsf{M}\boldsymbol{\xi} = 0, \tag{6}$$

where

$$\mathsf{M} = \begin{pmatrix}
\tilde{\lambda} & -2\Omega & 0 & -\frac{iF}{\rho\mu_0} & \frac{2\mu}{\rho\mu_0} & 0 & \frac{1}{\rho}\frac{d}{dr} \\
2\Omega + r\frac{d\Omega}{dr} & \tilde{\lambda} & 0 & -(2\mu + r\frac{d\mu}{dr}) & -\frac{iF}{\rho\mu_0} & 0 & \frac{1}{r\rho}im \\
0 & 0 & \tilde{\lambda} & 0 & 0 & -\frac{iF}{\rho\mu_0} & \frac{1}{\rho}ik \\
-iF & 0 & 0 & \tilde{\lambda} & 0 & 0 & 0 \\
r\frac{d\mu}{dr} & -iF & 0 & -r\frac{d\Omega}{dr} & \tilde{\lambda} & 0 & 0 \\
0 & 0 & -iF & 0 & 0 & \tilde{\lambda} & 0 \\
\frac{1}{r} + \frac{d}{dr} & \frac{im}{r} & ik & 0 & 0 & 0 & 0 \\
0 & 0 & 0 & \frac{1}{r} + \frac{d}{dr} & \frac{im}{r} & ik & 0
\end{pmatrix}, \tag{7}$$

with $\tilde{\lambda} = \lambda + im\Omega$ and $F = m\mu + B_z k$. We can eliminate from (7) the disturbance magnetic field to obtain the equations of $\tilde{\boldsymbol{u}}$ and $\tilde{p}$ as

$$\begin{aligned}
&\tilde{u_r} + \frac{1}{E\rho}\left(\tilde{\lambda} + \frac{F^2}{\tilde{\lambda}\rho\mu_0}\right)\frac{\mathrm{d}\tilde{p}}{\mathrm{d}r} + \frac{im}{E\rho r}\left(2\Omega - \frac{2i\mu F}{\tilde{\lambda}\rho\mu_0}\right)\tilde{p} = 0,\\
&\tilde{u_\theta} - \frac{1}{E\rho}\left[2\Omega + \left(1 + \frac{F^2}{\tilde{\lambda}^2\rho\mu_0}\right)r\frac{\mathrm{d}\Omega}{\mathrm{d}r} - \frac{2i\mu F}{\tilde{\lambda}\rho\mu_0}\right]\frac{\mathrm{d}\tilde{p}}{\mathrm{d}r}\\
&\qquad + \frac{im}{Er\rho}\left(\tilde{\lambda} + \frac{F^2}{\tilde{\lambda}\rho\mu_0} + \frac{2i\mu F}{\tilde{\lambda}^2\rho\mu_0}r\frac{\mathrm{d}\Omega}{\mathrm{d}r} - \frac{2\mu}{\tilde{\lambda}\rho\mu_0}r\frac{\mathrm{d}\mu}{\mathrm{d}r}\right)\tilde{p} = 0,\\
&\tilde{u_z} + \frac{ik}{\rho\left(\tilde{\lambda} + \frac{F^2}{\tilde{\lambda}\rho\mu_0}\right)}\tilde{p} = 0,
\end{aligned} \tag{8}$$

where

$$\begin{aligned}
E &= \left(\tilde{\lambda} + \frac{F^2}{\tilde{\lambda}\rho\mu_0}\right)^2 + \frac{2\mu r}{\tilde{\lambda}\rho\mu_0}\left(\tilde{\lambda} + \frac{F^2}{\tilde{\lambda}\rho\mu_0}\right)\left(\frac{iF}{\tilde{\lambda}}\frac{\mathrm{d}\Omega}{\mathrm{d}r} - \frac{\mathrm{d}\mu}{\mathrm{d}r}\right)\\
&\quad + 2\left[2\Omega + \left(1 + \frac{F^2}{\tilde{\lambda}^2\rho\mu_0}\right)r\frac{\mathrm{d}\Omega}{\mathrm{d}r} - \frac{2i\mu F}{\tilde{\lambda}\rho\mu_0}\right]\left(\Omega - \frac{i\mu F}{\tilde{\lambda}\rho\mu_0}\right).
\end{aligned} \tag{9}$$

With the expressions $\tilde{u_r}$, $\tilde{u_\theta}$ and $\tilde{u_z}$ in terms of $\tilde{p}$ at hand, we substitute (8) into the continuity equation (4), leaving the second order differential equation of $\tilde{p}$. By introducing a new variable $\chi = -ru_r/\tilde{\lambda}$ [13], we obtain, after some straightforward algebra, the second-order ordinary differential equation of χ again with the help of (8). This is no other than the Hain-Lüst equation [14], as extended to accommodate the effect of a rotating flow.

$$\frac{\mathrm{d}}{\mathrm{d}r}\left(f\frac{\mathrm{d}\chi}{\mathrm{d}r}\right) = g\chi, \tag{10}$$

where, by use of the definition $h^2 = m^2/r^2 + k^2$,

$$\begin{aligned}
f &= \frac{1}{h^2 r}\left(\tilde{\lambda}^2 + \frac{F^2}{\rho\mu_0}\right),\\
g &= \frac{\mathrm{d}}{\mathrm{d}r}\left(\frac{2im}{h^2r^2}\left(\Omega\tilde{\lambda} - \frac{i\mu F}{\rho\mu_0}\right)\right) + \frac{1}{r}\left(\tilde{\lambda}^2 + \frac{F^2}{\rho\mu_0}\right) + \frac{\mathrm{d}\Omega^2}{\mathrm{d}r} - \frac{1}{\rho\mu_0}\frac{\mathrm{d}\mu^2}{\mathrm{d}r} + \frac{4k^2\left(\Omega\tilde{\lambda} - \frac{\mu iF}{\rho\mu_0}\right)^2}{h^2 r(\tilde{\lambda}^2 + \frac{F^2}{\rho\mu_0})}.
\end{aligned}$$

We seek the solution of (10) in the WKB approximation. For this purpose, we substitute into (10) the form $\chi(r) = p(r)\exp[i\int q(r)\mathrm{d}r]$ with the constraint that the radial wavelength $2\pi/q$ is assumed to be much shorter than the characteristic length L, a measure for radial inhomogeneity, namely, $qL \gg 1$. Neglecting the second-order terms in $qL \gg 1$, the dispersion relation is gained from (10) as $q^2 = -g/f$, producing

$$\begin{aligned}
&(h^2 + q^2)\left(\tilde{\lambda}^2 + \frac{F^2}{\rho\mu_0}\right)^2 + 4k^2\left(\Omega\tilde{\lambda} - \frac{i\mu F}{\rho\mu_0}\right)^2\\
&+4h^2\left[\frac{imr}{2}\frac{\mathrm{d}}{\mathrm{d}r}\left(\frac{\Omega\tilde{\lambda} - \frac{i\mu F}{\rho\mu_0}}{h^2r^2}\right) + \Omega^2 Ro - \frac{\mu^2}{\rho\mu_0}Rb\right]\left(\tilde{\lambda}^2 + \frac{F^2}{\rho\mu_0}\right) = 0,
\end{aligned} \tag{11}$$

where we have introduced the Rossby number Ro and the magnetic Rossby number Rb by [5, 6]

$$Ro = \frac{1}{2}\frac{r}{\Omega}\frac{\mathrm{d}\Omega}{\mathrm{d}r}, \quad Rb = \frac{1}{2}\frac{r}{\mu}\frac{\mathrm{d}\mu}{\mathrm{d}r}. \tag{12}$$

3. Axisymmetric perturbations

For the standard MRI (SMRI), that is for $\boldsymbol{B} = B_z \boldsymbol{e}_z$, the maximum growth rate is the Oort A-value $\nu_A = \frac{1}{2}|\mathrm{d}\log\Omega/\mathrm{d}\log r| = |Ro|$ [7] which is attained at $m = 0$, the radial wavenumber $q = 0$ and the axial wavenumber k satisfying $\omega_A/\Omega = \pm\sqrt{1-\kappa^4/(16\Omega^4)}$, with $\omega_A = kB_z/\sqrt{\rho\mu_0}$ and κ being the epicyclic frequency [8, 9]. At the outset, we shall confirm that our approach of using (10) restores this well known result.

For the SMRI, the dispersion relation (11) simplifies, when $m = 0$, to

$$\frac{\lambda^2}{\Omega^2} + Ro\left(\frac{\lambda^2}{\Omega^2} + \frac{\omega_A^2}{\Omega^2}\right) + \frac{1}{4\alpha^2}\left(\frac{\lambda^2}{\Omega^2} + \frac{\omega_A^2}{\Omega^2}\right)^2 = 0, \tag{13}$$

where $\alpha = k/\sqrt{q^2+k^2}$. We read off from (13) limited to $\lambda = 0$ the stability boundary as

$$Ro_c = -\frac{\omega_A^2}{4\alpha^2\Omega^2} < 0. \tag{14}$$

As the magnetic field $\sqrt{k^2+q^2}B_z \to 0$, the above representation $Ro_c \to 0$. This is a resolution to the Velikhov-Chandrasekhar paradox [5], a glamour of the MRI. The eigenvalue λ, the root of (13), is

$$\frac{\lambda}{\Omega} = \pm\sqrt{\alpha^2 Ro^2 - \left(|\alpha| \mp \sqrt{\alpha^2(1+Ro)^2 + \left(\frac{\omega_A}{\Omega}\right)^2}\right)^2}. \tag{15}$$

The growth rate $\mathrm{Re}[\lambda]$, the real part of λ, reaches the maximum value $|\alpha Ro|$ at $(\omega_A/\Omega)^2 = \alpha^2[1-(1+Ro)^2]$, among which the maximum growth rate $\nu_\mathrm{A}/\Omega = |Ro|$, being the Oort A-value, is attained at $|\alpha| = 1$. It should be born in mind that the Oort A-value is realizable only when $-2 < Ro < 0$ as required by $(\omega_\mathrm{A}/\Omega)^2 > 0$ with k a disposable parameter. For a Keplerian rotation ($Ro = -3/4$), $\nu_\mathrm{A} = 3|\Omega|/4$ when $\omega_A = \pm\sqrt{15}\Omega/4$ in accord with ref [8]. The critical wavenumber for the instability is read off from (14) to be $\omega_A/\Omega = \pm\sqrt{-4Ro}$, meaning that the instability is invited when $\omega_A/\Omega \in (-\sqrt{-4Ro}, 0) \cup (0, \sqrt{-4Ro})$. For the SMRI, the most unstable mode is likely to be axisymmetric. The axisymmetric mode is tractable since the eigenvalues λ are either real or pure imaginary, whereas for a non-axisymmetric perturbation, the eigenvalues are complex, being less analytically tractable.

Next, we turn to the azimuthal MRI (AMRI), for which the magnetic field has an azimuthal component $\boldsymbol{B} = r\mu(r)\boldsymbol{e}_\theta$ only. For the axisymmetric case ($m = 0$), the growth rate calculated from (11) is

$$\lambda = \pm 2\Omega\alpha\sqrt{-1 - Ro + Rb\,\omega_{A\theta}^2/\Omega^2}, \quad \lambda = 0, \tag{16}$$

where $\omega_{A\theta} = \mu/\sqrt{\rho\mu_0}$, and $\lambda = 0$ is a double root. The instability region is $Ro < Rb\,\omega_{A\theta}^2/\Omega^2 - 1$, i.e., the critical Rossby number $Ro_c = Rb\,\omega_{A\theta}^2/\Omega^2 - 1$, which coincides with Knobloch's result [15]. In case of $Rb\,\omega_{A\theta} = 0$, the criterion reduces to that of Rayleigh's centrifugal instability; when either magnetic field or the magnetic shear vanishes, the Keplerian flow is stable. The magnetic shear acts to either lower ($Rb < 0$) or to raise ($Rb > 0$) the critical Rossby number for the axisymmetric mode. In view of (16), for a Keplerian flow ($Ro = -3/4$), the instability occurs for $Rb\,\omega_{A\theta}^2/\Omega^2 > 1/4$. Either increase of Rb on the side of $Rb > 0$ or $\omega_{A\theta}^2$ increases the growth rate.

4. Non-axisymmetric perturbations: weak external field

Inclusion of non-axisymmetric perturbations ($m \neq 0$) supplies rich characteristics of the AMRI. In order to gain an insight into the three-dimensional AMRI, we start with the stability analysis for a very weak magnetic field. We find that, when $|\omega_{A\theta}/\Omega| \ll 1$, the instability occurs for $Ro < Ro_c$, with a small value of Ro_c depending on Rb. This is similar to the case of the SMRI, for which $Ro_c(< 0)$ is given by (14) in the no-resistivity limit [6].

By trial and error of numerical calculation, it is probable that the maximum growth rate is attained in the limit of $k \to \infty$. The dispersion relation (11) reduces, in the limit of $k^2 + q^2 \to \infty$, to

$$4(\tilde{\lambda}\Omega - im\omega_{A\theta}^2)^2 + \frac{1}{\alpha^2}(\tilde{\lambda}^2 + m^2\omega_{A\theta}^2)^2 + (\tilde{\lambda}^2 + m^2\omega_{A\theta}^2)(4\Omega^2 Ro - 4Rb\,\omega_{A\theta}^2) = 0. \tag{17}$$

For motionless state ($\Omega \equiv 0$), the roots λ of (17) are written out explicitly in compact form as

$$\lambda = \pm\sqrt{-m^2 + 2\alpha^2 Rb \pm 2\alpha\sqrt{m^2 + \alpha^2 Rb^2}}\,\omega_{A\theta}. \tag{18}$$

At least one of the roots (18) becomes positive, signifying instability, when $2|\alpha|\sqrt{m^2 + \alpha^2 Rb^2} > m^2 - 2\alpha^2 Rb$. For an axisymmetric perturbation ($m = 0$), the instability criterion is $Rb > 0$. For non-axisymmetric perturbations, this condition is superseded by $Rb > m^2/(4\alpha^2) - 1$. A glance at (18) shows that the growth rate is zero for $\alpha = 0$. When m exhausts all the integral numbers and α exhausts all the real numbers contained in the range of $0 < |\alpha| \leq 1$, the magnetic Rossby number $Rb > -3/4$ is the widest possible Rb-range for instability, which coincides with the result, in the limit of $k \to \pm\infty$, derived by Newcomb's energy principle [12, 19]. Indeed, this condition coincides with the necessary condition for the instability expressed in the form

$$-rp' > \frac{1}{2\mu_0} m^2 \boldsymbol{B}^2, \tag{19}$$

where $p' = \mathrm{d}p/\mathrm{d}r$ [13]. Substituting $\boldsymbol{B}(r) = B_\theta(r)\boldsymbol{e}_\theta$ into the equilibrium condition $\boldsymbol{0} = -\nabla p + (\nabla \times \boldsymbol{B}) \times \boldsymbol{B}/\mu_0$, we have, $p' = -B_\theta/(\mu_0 r)(rB_\theta)'$. As noted in ref [13], (19) is not valid for the axisymmetric case $m = 0$, for which (19) is taken place of by Suydam's criterion for the local interchange condition. As a consequence, $m = \pm 1$ in (19) provides the maximum possible range for instability, and this condition is exactly $Rb > -3/4$.

The maximum growth rate is found by rewriting (18) as

$$\lambda = \pm\sqrt{\alpha^2(Rb + 1)^2 - \left(\sqrt{m^2 + \alpha^2 Rb^2} \mp \alpha\right)^2}\,\omega_{A\theta}. \tag{20}$$

Since m takes integral values but α is confined to the range $0 < |\alpha| \leq 1$, the maximum of λ is attained either at $m = 0$ or $m = \pm 1$. When Rb is larger than $3/4$, the maximum is $\lambda_{\max} = 2\sqrt{Rb}|\omega_{A\theta}|$ attained at $m = 0$ and $|\alpha| = 1$. For $-3/4 < Rb \leq 3/4$, the maximum is attained at $m = \pm 1$ with its value $\lambda_{\max} = \sqrt{-1 + 2Rb + 2\sqrt{1 + Rb^2}}|\omega_{A\theta}|$.

Next, we touch upon the eigenvalues of waves in a rotating flow with no external magnetic field. For a non-axisymmetric perturbation $m \neq 0$ and simultaneously in the presence of a rotational flow with angular velocity $\Omega \neq 0$, the energy principle is difficult to apply, and we appeal to the WKB method by restricting to short-wavelength perturbations. In the absence of magnetic field ($\omega_{A\theta} \equiv 0$), (17) has roots $\lambda_{1,2}/\Omega = -im \pm 2\alpha\sqrt{-(1 + Ro)}$ and

$\lambda_{3,4}/\Omega = -im$. The latter pertain to the mode characterized by the advection of the disturbance magnetic field frozen into the local rotating flow. The root $\lambda_{1,2}$ pertain to the inertial wave or the Kelvin wave [20]. Its frequency $\omega_{1,2}$ as defined by $\lambda_{1,2} = -i\omega_{1,2}$ is given by $\omega_{1,2} = m \mp 2\alpha\sqrt{1+Ro}$. This distinction between $\lambda_{1,2}$ and $\lambda_{3,4}$ manifests itself by constructing the eigenfunction $\boldsymbol{\xi}$ of (6). For simplicity, we take $Ro = 0$, $\alpha = 1$ and $|m| \ll |k|$. The eigenfunctions corresponding to $\lambda_{1,2} = -i(m \mp 2)$ are $\boldsymbol{\xi}_{1,2} = (\mp i, 1, 0, 0, 0, 0, 0)$, and those corresponding to $\lambda_{3,4} = -i\omega_{3,4}$ are $\boldsymbol{\xi}_3 = (0, 0, 0, 1, 0, 0, 0)$ and $\boldsymbol{\xi}_4 = (0, 0, 0, 0, 1, 0, 0)$. It is simply the disturbance magnetic field $\boldsymbol{\xi}_{3,4}$ that is advected by the fluid ($\omega_{3,4} = m$). For a uniform rotation ($Ro = 0$), the frequency $\omega_{1,2} = m \mp 2\alpha$ is confined to $-2 \le \omega_1 \le 0$ (upper sign) and $0 \le \omega_2 \le 2$ (lower sign) [21]. The parameter α plays the role of a counter for the radial nodal structure, with $|\alpha| = 1$, or $|q/k| \ll 1$, corresponding to a simple structure and with $|\alpha| \ll 1$, or $|q/k| \gg 1$, corresponding to a highly fine radial structure. The mode with eigenfrequecy ω_1, being smaller than $m\Omega$, is called the retrograde mode, while the one with eigenfrequecy ω_2, being larger than $m\Omega$, is called the cograde mode [20]. Alternatively, from the viewpoint of the way approaching the limiting frequency m for $\alpha = 0$, ω_1 and ω_2 are referred to as the Sturmian and the anti-Sturmian, respectively [14]. There is no growing perturbation unless $Ro < -1$. This implies that the same criterion as Rayleigh's one for the centrifugal instability applies to the non-axisymmetric perturbations too. Fig. 1 depicts $\mathrm{Re}[\lambda]$ (left) and $\mathrm{Im}[\lambda] = -\omega$ (right) of the eigenvalue for the helical perturbation $m = 1$ with the simplest nodal structure $\alpha = 1$ when no external magnetic field is applied ($\omega_{A\theta} \equiv 0$).

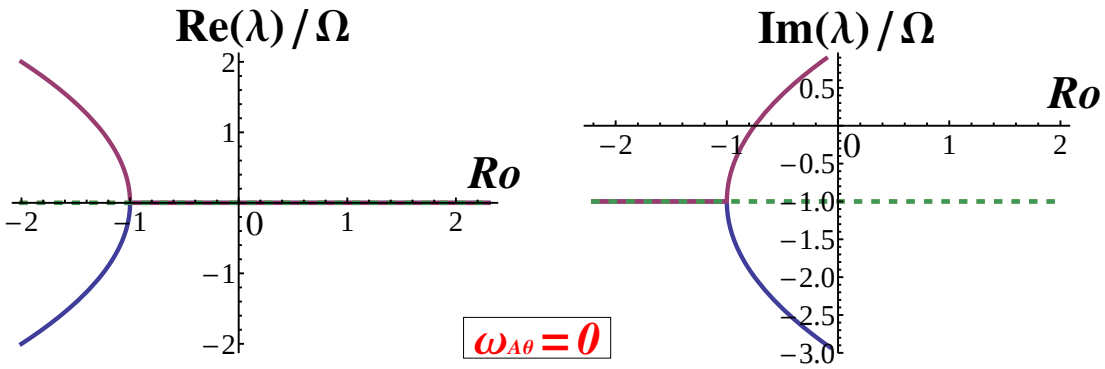

Fig. 1 The growth rate $\mathrm{Re}[\lambda]$ (left) and the frequency $\mathrm{Im}[\lambda] = -\omega$ (right) of the perturbation of $m = 1$ and $\alpha = 1$ in the absence of the external magnetic field ($\omega_{A\theta} \equiv 0$ and consequently $Rb = 0$).

We are now ready to inquire into how a weak azimuthal magnetic field deforms the above dispersion relation. When $\omega_{A\theta} \neq 0$, but with $|\omega_{A\theta}/\Omega| \ll 1$, the expression for the eigenvalue

can be expanded to second order in a small parameter $\omega_{A\theta}/\Omega$ as, unless $|\alpha| \ll 1$,

$$\frac{\lambda_{1,2}}{\Omega} \approx \begin{cases} -im \pm 2|\alpha|\sqrt{-(1+Ro)} - \dfrac{1}{1+Ro}\Bigg(im \pm Rb|\alpha|\sqrt{-(1+Ro)} \\ \qquad \pm \dfrac{m^2}{4|\alpha|}\dfrac{2+Ro}{\sqrt{-(1+Ro)}}\Bigg)\left(\dfrac{\omega_{A\theta}}{\Omega}\right)^2 & (Ro \neq -1), \\ -im \pm \sqrt{\dfrac{2\alpha m\omega_{A\theta}}{\Omega}} + i\dfrac{\alpha\omega_{A\theta}}{\Omega} \pm \dfrac{\alpha^2 - m^2 + \alpha^2 Rb}{2\sqrt{2\alpha m}}\left(\dfrac{\omega_{A\theta}}{\Omega}\right)^{3/2} & (Ro = -1), \end{cases} \tag{21}$$

$$\frac{\lambda_{3,4}}{\Omega} \approx \begin{cases} -im \pm m\sqrt{\dfrac{Ro}{-(1+Ro)}}\dfrac{\omega_{A\theta}}{\Omega} + \dfrac{im}{1+Ro}\left(\dfrac{\omega_{A\theta}}{\Omega}\right)^2 & (Ro \neq -1, 0), \\ -im \pm i\sqrt{\dfrac{2\alpha m\omega_{A\theta}}{\Omega}} - i\dfrac{\alpha\omega_{A\theta}}{\Omega} \mp i\dfrac{\alpha^2 - m^2 + \alpha^2 Rb}{2\sqrt{2\alpha m}}\left(\dfrac{\omega_{A\theta}}{\Omega}\right)^{3/2} & (Ro = -1), \\ -im + m\left(i \mp \sqrt{Rb - m^2/(4\alpha^2)}\right)\left(\dfrac{\omega_{A\theta}}{\Omega}\right)^2 & (Ro = 0), \end{cases} \tag{22}$$

where the double-sign corresponds, and the upper sign corresponds to λ_1 and λ_3, and the lower sign corresponds to λ_2 and λ_4. For both $\lambda_{1,2}$ and $\lambda_{3,4}$, the first expansions are singular at $Ro = -1$, where a separate treatment is necessary. For the expansion at $Ro = -1$, we have ignored terms of $O\left((\omega_{A\theta}/\Omega)^2\right)$. For $\lambda_{3,4}$, the first expansion for $Ro \neq -1, 0$ of (22) is invalidated in the limit of $Ro \to 0$ as well, because the coefficient of the third term $(\omega_{A\theta}/\Omega)^3$ is proportional to $Ro^{-1/2}$, which diverges in the limit $Ro \to 0$. This singularity requires a separate treatment for the case of $Ro = 0$ and the resulting expression is the third expression of (22). The branches $\lambda_{1,2}$ of the inertial waves, subjected to the azimuthal magnetic field, are called the fast magneto-Coriolis (MC) waves. The branches $\lambda_{3,4}$ are called the slow magneto-Coriolis (MC) waves [6]. In case of $|\alpha| \ll 1$, (21) and (22) give way to

$$\frac{\lambda_{1,2}}{\Omega} \approx -im\left(1 + \frac{\omega_{A\theta}}{\Omega}\right) \pm i\left(1 + \frac{\omega_{A\theta}}{\Omega}\right)|\alpha| + O(\alpha^2), \tag{23}$$

$$\frac{\lambda_{3,4}}{\Omega} \approx -im\left(1 - \frac{\omega_{A\theta}}{\Omega}\right) \pm i\left(1 - \frac{\omega_{A\theta}}{\Omega}\right)|\alpha| + O(\alpha^2). \tag{24}$$

By applying the magnetic field, the frequency m degenerate at $\alpha = 0$ is split into $m(1 \pm \omega_{A\theta}/\Omega)$. In the limit of $|\alpha| \to 0$, the frequency defined via $\lambda_{1,2} = -i\omega_{1,2}$ of the fast MC waves degenerate to $m(\Omega + \omega_{A\theta})$ with ω_1 (upper sign) approaching from below and ω_2 (lower sign) from above, and that of the slow MC waves, stemming from the frozen-in advection, degenerate to $m(\Omega - \omega_{A\theta})$with ω_3 (upper sign) approaching from below and ω_4 (lower sign) from above. For this reason, the fast and slow MC waves may refer to the forward and the backward modes, with the upper sign Sturmian and the lower sign anti-Sturmian [14].

The first expansion of (22) suggests that the instability occurs when $Ro \lesssim 0$. This property is reminiscent of the SMRI for which the critical Rossby number (14) is close to but less than zero if the resistivity is zero [6]. The situation is slightly different for the AMRI. The first of (22) becomes invalid at $Ro = 0$, to which the third expansion of (22) applies. The third one implies that, when $Rb > m^2/(4\alpha^2) \geq m^2/4$ by varying $|\alpha| \in (0, 1]$, $Ro_c > 0$, but otherwise, $Ro_c \leq 0$. In the following, we determine Ro_c

Since Ro_c is very small, we seek a series solution, in small parameter $\omega_{A\theta}/\Omega$, of (17) not only for λ but also for Ro. The result for the slow MC wave is

$$\begin{aligned} Ro &\approx Ro_2\left(\omega_{A\theta}/\Omega\right)^2 + \cdots, \\ \frac{\lambda_{3,4}}{\Omega} &\approx -im + m\left(i \pm \sqrt{Rb - Ro_2 - m^2/(4\alpha^2)}\right)\left(\frac{\omega_{A\theta}}{\Omega}\right)^2, \end{aligned} \tag{25}$$

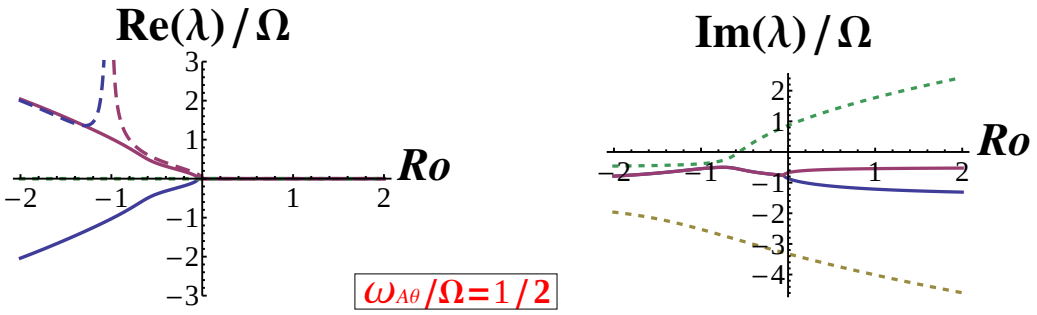

Fig. 2 The growth rate Re[λ] (left) and the frequency Im[λ] = $-\omega$ (right) of the perturbation of $m = 1$ and $\alpha = 1$ for $\omega_{A\theta}/\Omega = 0.5$. The magnetic shear is $Rb = 0$. The long dashed lines (left) draw the positive real part of the first of (21) for $Ro < -1$ and that of (22) for $-1 < Ro < 0$.

for $0 < |\alpha| \leq 1$. It follows from (25) that the slow MC wave is amplified when $Ro_2 < Rb - m^2/(4\alpha^2)$. For small values of $(\omega_{A\theta}/\Omega)^2$, the AMRI is caused when approximately

$$Ro < \left(Rb - \frac{m^2}{4\alpha^2}\right)\left(\frac{\omega_{A\theta}}{\Omega}\right)^2 \leq Ro_c \approx \left(Rb - \frac{1}{4}\right)\left(\frac{\omega_{A\theta}}{\Omega}\right)^2. \tag{26}$$

Fig. 2 draws the growth rate (left) and the frequency (right) for $\omega_{A\theta}/\Omega = 0.5$. The other parameters $m = 1$, $\alpha = 1$ and $Rb = 0$ are common with Fig. 1. For this choice of the parameters, $Ro_c = -1/16$. It is observed that the instability is driven when the frequencies ω_3 and ω_4 of the slow MC wave (= backward wave) collide at around $\omega = m = 1$ at the critical value Ro_c. To clarify the source for the instability, the positive values of the asymptotic formulas Re[$\lambda_{1,2}/\Omega$] and Re[$\lambda_{3,4}/\Omega$] provided by the first equations of (21) and (22) respectively are superposed, with long dashed lines, on the left of Fig. 2. For $Ro > -1$, the instability originates from the slow MC waves, but, for $Ro < -1$, the dominant role in the instability is played by the fast MC waves. At the dividing point $Ro = -1$, the flow is necessarily unstable; for $\alpha m \omega_{A\theta}/\Omega > 0$, Re[$\lambda_{1,2}$] $\neq 0$ as is seen from the second of (21) and the fast MC wave is amplified, but, for $\alpha m \omega_{A\theta}/\Omega < 0$, the slow MC wave is amplified, with growth rate given by |Re[$\lambda_{3,4}$]|, the real part of the second of (22).

Here we point out that, unlike the axisymmetric SMRI, the axisymmetric AMRI is of the fast MC-wave origin. The growth rate of the axisymmetric AMRI, the left values of (16) in the limit of $k \to \infty$, has a link with the first of (21) specialized to $m = 0$. For the fast MC wave, the critical Rossby number Ro_c is close to -1 when $|\omega_{A\theta}/\Omega| \ll 1$, being in consistent with the argument of §3. On the contrary, the eigenvalues (22) of the slow MC wave become zero for $m = 0$, in agreement with the second values of (16), which does not contribute to the axisymmetric AMRI. For the AMRI, the slow MC wave, raising the critical value to $Ro_c \approx 0$, close to Velikhov-Chandrasekhar's value for the SMRI, is intrinsic to non-axisymmetric perturbations.

Given a small value of $|\omega_{A\theta}/\Omega|$, the maximum growth rate increases with $|m|$. Interestingly, the maximum growth rate approaches, as $|m|$ is increased, the same value as that of the SMRI. Fig. 3 displays the growth rate ν = Re[$\lambda_{3,4}$] as functions of the Alfvén frequency $\omega_{A\theta}$ with azimuthal wavenumbers $m = 1$, 5 and 10 for $Ro = -3/4$ and $Rb = -1$. Since the system

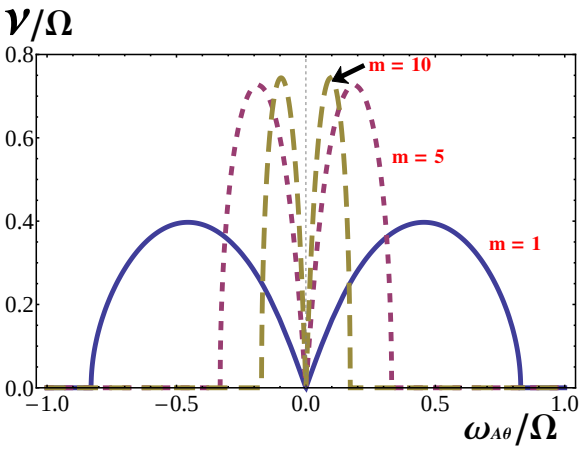

Fig. 3 The growth rate, in the limit $k \to \infty$ with fixing $\alpha = 1$, of the non-axisymmetric AMRI versus $\omega_{A\theta}/\Omega$, in the range of small values, for different azimuthal wavenumbers $m = 1$ (solid line), 5 (dashed line) and 10 (long dashed line) for $Ro = -3/4$, a Keplerian rotation. The magnetic Rossby number is $Rb = -1$.

is Hamiltonian, to each damping perturbation ($\nu < 0$) corresponds the growing perturbation ($\nu > 0$) and therefore we display only the solution with positive real part ν. The change of the sign of Rb, namely, the choice of $Rb = 1$, does not change much the growth rate. We observe from Fig. 3 that, as m increases, the maximum growth rate approaches $3|\Omega|/4$, though the width of the instability band in $\omega_{A\theta}/\Omega$ becomes narrow with m. Indeed, by taking $m\omega_{A\theta}^2 = 0$ and $Rb\omega_{A\theta}^2 = 0$ in (17) as a limit of small values of $|\omega_{A\theta}/\Omega|$ with maintaining $|m\omega_{A\theta}/\Omega|$ finite, we can show that the maximum growth rate happens to coincides with the Oort A-value $\nu_{\rm A}/|\Omega| = |Ro|$. In this limit, (17) is solved for $\tilde{\lambda}$, yielding

$$\frac{\lambda}{\Omega} = -im \pm \sqrt{\alpha^2 Ro^2 - \left(\sqrt{\left(m\frac{\omega_{A\theta}}{\Omega}\right)^2 + \alpha^2(1+Ro)^2} \mp \alpha\right)^2}. \tag{27}$$

The growth rate $\nu = |\mathrm{Re}[\lambda]|$ takes the maximum value close to $|\alpha Ro|$ when $\sqrt{(m\omega_{A\theta}/\Omega)^2 + \alpha^2(1+Ro)^2} = |\alpha|$, or at $m \approx \pm(\Omega/\omega_{A\theta})\alpha\sqrt{1-(1+Ro)^2}$. Actually m should be an integer closest to the right hand side. By varying α, the maximum value among the above is close to the Oort A-value $\nu_{\rm A}/|\Omega| = |Ro|$ at $\alpha = \pm 1$ [7]. The instability window is found from (27) as $\alpha^2 Ro^2 > (\sqrt{(m\omega_{A\theta}/\Omega)^2 + \alpha^2(1+Ro)^2} - |\alpha|)^2$. The instability takes place for $0 < |\omega_{A\theta}/\Omega| < 2\sqrt{|\alpha Ro|}/|m|$, whose upper bound $2\sqrt{|Ro|}/|m|$ is reached at $|\alpha| = 1$, The width of the instability band is narrowed with $|m|$ in inversely proportional to $|m|$ as is confirmed from Fig. 3.

The AMRI shares common features with the SMRI that the instability occurs for $Ro < Ro_c \approx 0$ however weak the external magnetic field may be, when it is applied, and the maximum growth rate is $|Ro|$, regardless of strength of the external field. This resemblance holds true as far as $|\omega_{A\theta}/\Omega| \ll 1$. However, a distinctive behavior manifests itself when the azimuthal magnetic field B_θ is intensified to the level $|\omega_{A\theta}/\Omega| = O(1)$ as will be described in the subsequent section.

5. Non-axisymmetric perturbations: strong external field

This section is concerned with the case of $|\omega_{A\theta}/\Omega| \sim 1$. Above all, we shall show that, when $Rb > -3/4$, the both cases $Ro < 0$ and $Ro \geq 0$ entail the instability with unstable mode excited at $|k| \to \infty$, or, put another way, there is no critical Rossby number. But this mode subsides down as Rb is decreased and dies down at $Rb = -3/4$. Instead, another unstable mode of $k = 0$ is born at $Rb = -1/4$, develops as Rb is decreased, and surpasses the mode of $|k| \to \infty$ for $Rb \leq -1/\sqrt{8}$. The instability mode of $k = 0$ is confined to a finite range in Ro centered on $Ro = 0$, $Ro^2 < (|Rb| - 1/4)(\omega_{A\theta}/\Omega)^2$ for $-1/2 \leq Rb < -1/4$, and $Ro^2 < Rb^2(\omega_{A\theta}/\Omega)^2$ for $Rb < -1/2$. We should keep in mind the results of the previous section that, for small value of $|\omega_{A\theta}/\Omega|$, the unstable mode of $|k| \to \infty$ prevails for the entire range of Rb, though restricted to $Ro < Ro_c$, with Ro_c depending on Rb as given by (26).

The numerical calculation for $m = 1$, for instance, shows that, for $Rb > 0$, the maximum growth rate is taken in the limit of $k \to \infty$ and that the maximum value overshoots the Oort A-value $\nu_{\rm A}$ when $|\omega_{a\theta}|$ and Rb are increased. In the limit of $k \to \infty$ with fixing α, the asymptotics of the growth rate for $|\omega_{A\theta}/\Omega| \gg 1$ is deduced with ease by manipulating the expansion of (17) in $\Omega/\omega_{A\theta}$, up to $O((\Omega/\omega_{A\theta})^0)$, as

$$\frac{\lambda_{1,2}}{\Omega} \approx \pm\sqrt{2\alpha^2 Rb - m^2 + 2|\alpha|\sqrt{m^2 + \alpha^2 Rb^2}}\frac{\omega_{A\theta}}{\Omega} - im\left(1 - \frac{|\alpha|}{\sqrt{m^2 + \alpha^2 Rb^2}}\right), \quad (28)$$

$$\frac{\lambda_{3,4}}{\Omega} \approx \pm\sqrt{2\alpha^2 Rb - m^2 - 2|\alpha|\sqrt{m^2 + \alpha^2 Rb^2}}\frac{\omega_{A\theta}}{\Omega} - im\left(1 + \frac{|\alpha|}{\sqrt{m^2 + \alpha^2 Rb^2}}\right). \quad (29)$$

The parameter Ro resides only in higher-order terms in $\Omega/\omega_{A\theta}$. The both sides of $Ro < 0$ and $Ro \geq 0$ entail the instability, as opposed the case of small values of $|\omega_{A\theta}/\Omega|$. When $Rb > 0$, (28) and (29) are reduced, if specialized to $m = 0$, to the large $\omega_{A\theta}/|\Omega|$ asymptotics of the left and the right of (16). Unlike the case of $|\omega_{A\theta}/\Omega| \ll 1$, the unstable mode is necessarily the fast MC wave ($\lambda_{1,2}$) regardless of the value of Ro. When $Rb < 0$, the roles of $\lambda_{1,2}$ and $\lambda_{3,4}$ are exchanged. The growth rate is proportional to $\omega_{A\theta}/\Omega$. The maximum value of the growth rate $\nu_{1,2} = {\rm Re}[\lambda_{1,2}]$ with respect to m and α is evaluated by rewriting (28) into

$$\frac{\nu_{1,2}}{\Omega} \approx \pm\sqrt{\alpha^2(Rb+1)^2 - \left(\sqrt{m^2 + \alpha^2 Rb^2} - |\alpha|\right)^2}\frac{\omega_{A\theta}}{\Omega}. \quad (30)$$

For an integer m and $0 < |\alpha| \leq 1$, this is real when $Rb \geq m^2/(4\alpha^2) - 1 \geq -3/4$ ($m \neq 0$) and $Rb \geq 0$ ($m = 0$). The maximum value is taken at $|\alpha| = 1$, and at $m = 0$ for $Rb \geq 3/4$, but at $|m| = 1$ for $-3/4 < Rb < 3/4$, with the maximum values

$$\frac{\nu_{\rm max}}{\Omega} \approx \begin{cases} 2\sqrt{Rb}|\omega_{A\theta}/\Omega| & (Rb \geq 3/4), \\ \sqrt{2Rb - 1 + 2\sqrt{1 + Rb^2}}|\omega_{A\theta}/\Omega| & (-3/4 < Rb < 3/4). \end{cases} \quad (31)$$

This value decreases to zero as Rb decreases to $-3/4$.

Fig. 4 shows the growth rate, for $m = 1$ in the limit of $k \to \infty$, over a wide range of the Alfvén frequency $\omega_{A\theta}/\Omega$ and for typical values of Rb ($= 0,\ 1,\ 5$) in the range of $Rb - 3/4$. The flow is Keplerian ($Ro < 0$). Fig. 5 is the counterpart for positive $Ro(= 1)$. The difference lies in the neighborhood of the origin $(\omega_{A\theta}/\Omega, \nu/\Omega) = (0, 0)$. The critical condition (26), if rearranged, implies that, for $Rb > 1/4$, the unstable mode of $|k| \to \infty$ is excited for $(\omega_{A\theta}/\Omega)^2 > Ro/(Rb - 1/4)$, though the validity is limited to $|\omega_{A\theta}/\Omega| \ll 1$. Fig. 5 for $Ro > 0$ exhibits the disappearance of instability in a finite range in $|\omega_{A\theta}/\Omega|$, being wider for a smaller

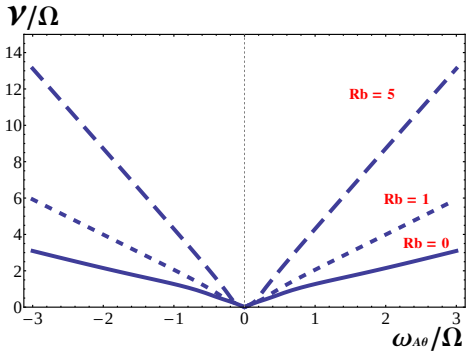

Fig. 4 The growth rate, for $m = 1$ and $k \to \infty$ with fixing $\alpha = 1$, of the non-axisymmetric AMRI over a wide range of $\omega_{A\theta}/\Omega$ for negative $Ro = -3/4$ and different non-negative magnetic Rossby numbers Rb: $Rb = 0$ (solid line), 1 (dashed line) and 5 (long dashed line).

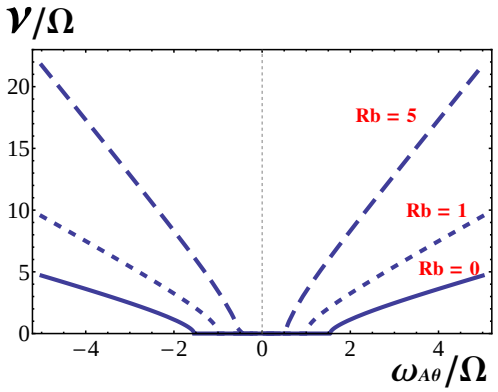

Fig. 5 The growth rate, for $m = 1$ and $k \to \infty$, of the non-axisymmetric AMRI over a wide range of $\omega_{A\theta}/\Omega$ for positive $Ro = 1$ and different non-negative Rb: $Rb = 0$ (solid line), 1 (dashed line), 5 (long dashed line).

value of Rb ($> 1/4$). For instance, the $k \to \infty$ mode arises at $\omega_{A\theta}/\Omega \approx 0.48$ for $Ro = 1$ and $Rb = 5$, for which $\sqrt{Ro/(Rb - 1/4)} \approx 0.4588$.

An unstable mode of the other extreme $k \to 0$ is seeded at $Rb = -1/4$, is strengthened and becomes dominant as Rb is decreased on the side of $Rb < 0$ and $|\omega_{A\theta}/\Omega| \sim 1$. In this limit, the dispersion relation (11) admits its roots in a tidy form as

$$\begin{aligned} \frac{\lambda}{\Omega} &= \frac{-im(m^2 + q^2r^2 + 2Ro) \pm m\sqrt{(-4Rb - m^2 - q^2r^2)(m^2 + q^2r^2)(\omega_{A\theta}/\Omega)^2 - 4Ro^2}}{m^2 + q^2r^2}, \\ \frac{\lambda}{\Omega} &= -im\left(1 \pm \frac{\omega_{A\theta}}{\Omega}\right). \end{aligned} \tag{32}$$

The instability is driven when $-4Rb - m^2 - q^2r^2 > 0$ with $m \neq 0$, namely, $Rb < -(m^2 + q^2r^2)/4 \leq -1/4$. The possible real part ν of the first of (32) reads

$$\frac{\nu}{\Omega} = \pm\frac{m}{m^2 + q^2r^2}\sqrt{[4Rb^2 - (m^2 + q^2r^2 + 2Rb)^2]\left(\frac{\omega_{A\theta}}{\Omega}\right)^2 - 4Ro^2}. \tag{33}$$

It follows from (33) that the sign of Ro is irrelevant to the growth rate, The instability occurs in a finite range in Ro centered on $Ro = 0$. Noting that the realizability of $m^2 + q^2r^2 + 2Rb = 0$ for $m \neq 0$ is confined to $Rb \leq -1/2$, the maximum width of the instability band is obtained, for $-1/2 \leq Rb < -1/4$, by taking $|m| = 1$ and $q = 0$, with the instability range $Ro^2 < (|Rb| - 1/4)(\omega_{A\theta}/\Omega)^2$. For $Rb < -1/2$, the instability range is $Ro^2 < Rb^2(\omega_{A\theta}/\Omega)^2$, and the large-magnetic-field asymptotics of the growth rate ν is obtained from (33) as

$$\frac{\nu}{\Omega} \approx \sqrt{\frac{4|Rb|}{m^2 + q^2r^2} - 1}\left|\frac{m\omega_{A\theta}}{\Omega}\right| \leq \sqrt{4|Rb| - 1}\left|\frac{\omega_{A\theta}}{\Omega}\right|, \tag{34}$$

with the upper bound taken at $q = 0$ and $|m| = 1$. Comparison with (31) shows that the instability mode of $k = 0$ prevails over that of $|k| \to \infty$ for approximately $Rb \leq -1/\sqrt{8}$.

The condition $1 \leq m^2 + q^2r^2 < -4Rb$, under restriction of $m \neq 0$, for existence of the unstable mode of $k = 0$ signifies that the value of $|Rb|$ limits the range of $|m|$ for instability. For

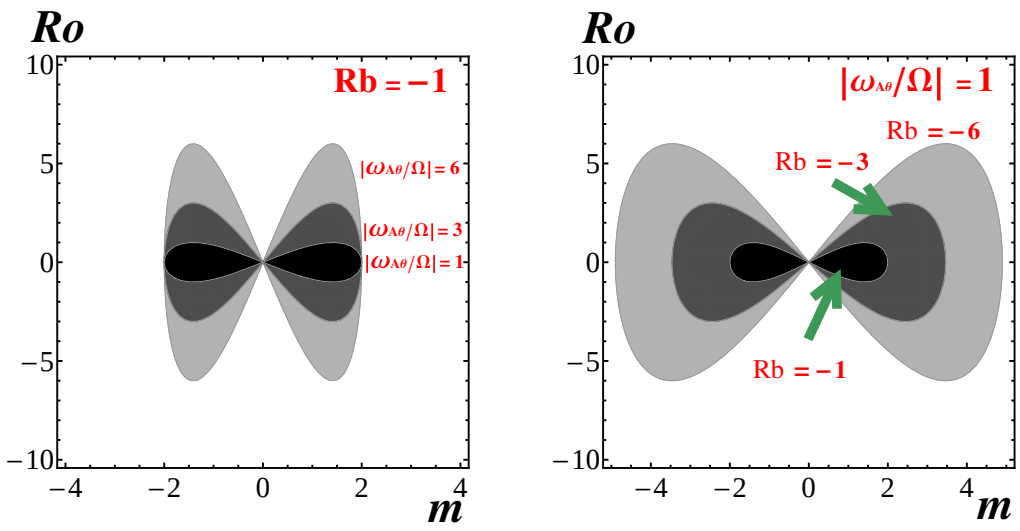

Fig. 6 The instability region of the non-axisymmetric wave of $k = 0$ for $Rb < -1/4$. The flow is Keplerian ($Ro = -3/4$). The left figure fixes $Rb = -1$ and depicts the instability region with increasing $|\omega_{A\theta}(r)/\Omega|$ from dark gray to light gray. The right figure fixes $|\omega_{A\theta}(r)/\Omega| = 1$ and depicts the instability region with increasing $|Rb|$ from dark gray to light gray.

instance, $Rb = -1$ admits only $m = \pm 1$ for instability. To have an idea of the instability parameters for the case of $Rb < -1/4$ and $|\omega_{A\theta}/\Omega| \sim 1$, we draw in Fig. 6 the instability region, in the space of (m, Ro), of the $k = 0$ wave, for a Keplerian flow ($Ro = -3/4$). The left of Fig. 6 fixes $Rb = -1$ and varies the values of $|\omega_{A\theta}/\Omega|$. The right fixes $|\omega_{A\theta}/\Omega| = 1$ and varies the values of Rb. The gray region indicates the set of parameters for which the AMRI occurs, painted with darker gray as the parameter value is increased. Fig. 6 shows that the increase of $|\omega_{A\theta}(r)/\Omega|$ and/or $|Rb|$ enlarges the instability range in Ro, though limited the case of $Rb < -1/4$ with $|\omega_{A\theta}/\Omega| \sim 1$. The left figure confirms that Rb determines the range of azimuthal wavenumber m for the instability. The right figure shows that increases in $|Rb|$ results in widening of the instability range both in Ro and m.

For $Rb \geq -1/\sqrt{8}$, the shortest waves ($k \to \infty$) dominate over the long waves ($k = 0$) for $|\omega_{A\theta}/\Omega| \sim 1$, and the transition of behavior from the regime of $|\omega_{A\theta}/\Omega| \ll 1$ to the regime $|\omega_{A\theta}/\Omega| \sim 1$ is displayed in a single figure Fig. 4 for the case of $Ro \leq 0$ and in Fig. 5 for the case of $Ro > 0$. A distinctive feature of Fig. 5 arises around the origin $(\omega_{A\theta}/\Omega, \nu/\Omega) = (0, 0)$, where the instability disappears in a finite range of $\omega_{A\theta}/\Omega$ with its width depending on Rb. Notably, the maximum growth rate increases, beyond the Oort A-value, indefinitely with $|\omega_{A\theta}/\Omega|$ linearly in it.

On the other hand, a smooth transition may not be expected from the regime of $|\omega_{A\theta}/\Omega| \ll 1$ to that of $|\omega_{A\theta}/\Omega| \sim 1$, when $Rb < -1/\sqrt{8}$, because the maximum growth rate occurs in the short-wave limit ($k \to \infty$) for $|\omega_{A\theta}/\Omega| \ll 1$, but in the long-wave limit for $|\omega_{A\theta}/\Omega| \sim 1$. With a choice of $Ro = -3/4$ and $Rb = -1/2$, Fig. 7 draws the maximum growth rate of $m = 1$ mode, in the limit of $k \to \infty$ and in the opposite limit $k \to 0$ simultaneously. For the

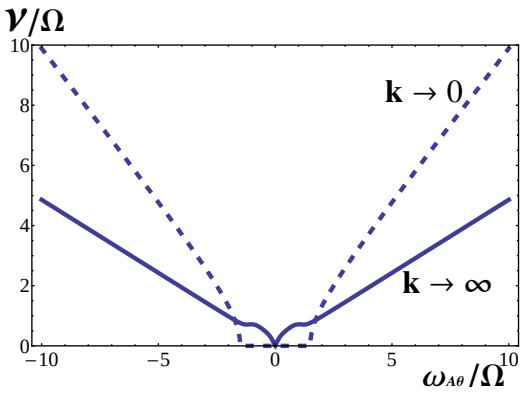

Fig. 7 The crossover of the most unstable mode of $m = 1$ from the regime of $|\omega_{A\theta}/\Omega| \ll 1$ to that of $|\omega_{A\theta}/\Omega| \sim 1$ in the case of $Rb = -1/2$. The maximum growth rates occurs at $k \to \infty$ (solid line) in the former regime but at $k = 0$ in the latter (dashed line), and they are simultaneously drawn as a function of $\omega_{A\theta}/\Omega$. The flow is Keplerian ($Ro = -3/4$). In the both limits, the maxima are taken at $|\alpha| = 1$.

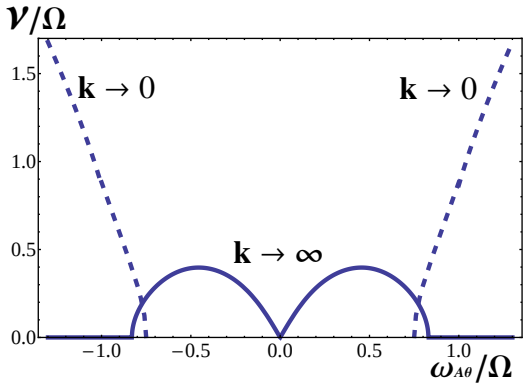

Fig. 8 The crossover of the most unstable mode of $m = 1$ from the regime of $|\omega_{A\theta}/\Omega| \ll 1$ to that of $|\omega_{A\theta}/\Omega| \sim 1$ in the case of $Rb = -1$ for a Keplerian flow ($Ro = -3/4$). For the limit of $k = 0$, $|qr| = 1$ at the critical point $\omega_{A\theta}/\Omega = 3/4$ and $|qr|$ decreases, with $\omega_{A\theta}/\Omega$, to zero along the graph.

former, the maximum occurs at $|\alpha| = 1$ and for the latter, the maximum occurs at $q = 0$, being mathematically equivalent to each other. As argued above, because $Rb < -1/\sqrt{8}$, the mode of $k \to 0$ overweighs that of $k \to \infty$ in the regime of $|\omega_{A\theta}/\Omega| \sim 1$. The maximum growth rate of the former increases without bound in proportion to $|\omega_{A\theta}/\Omega|$. The instability mode of $k = 0$, being admitted only for $|\omega_{A\theta}/\Omega| > |Ro/Rb| = |Ro|/\sqrt{|Rb| - 1/4} = 3/2$ when $Rb = -1/2$, is excluded in the regimes of $|\omega_{A\theta}/\Omega| \ll 1$

Fig. 8 chooses $Rb = -1$, with the other parameters being unchanged. In the regime $|\omega_{A\theta}/\Omega| \ll 1$ accommodates the instability modes of $|k| \to \infty$ with $|m| \geq 2$ with the overall maximum growth rate being close to the Oort A-value, as illustrated by Fig. 3. In the regime $|\omega_{A\theta}/\Omega| \sim 1$, the instability mode of $k \to \infty$ disappears because $Rb \leq -3/4$. The maximum growth rate for $k \to \infty$ corresponds to $|\alpha| = 1$. But this is not the case with the wave of $k = 0$. Near the critical point $|\omega_{A\theta}/\Omega| = |Ro/Rb| = 3/4$, the most unstable mode has $|qr| = 1$ in favor of $m^2 + q^2r^2 + 2Rb = 0$. As $|\omega_{A\theta}/\Omega|$ is increased, $|qr|$ decreases monotonically to zero as is seen from (34). In between, the maximum is taken at an intermediate value of qr. On the whole, for $|\omega_{A\theta}/\Omega| \gtrsim 0.8$ approximately, the mode of $k = 0$ prevails over that of $k \to \infty$. For $Ro = -3/4$ and $Rb = -1$, we draw in Fig. 9 the growth rate ν as a function of the radial wavenumber qr. The maximum growth rate is found with ease to be $\nu_{\max}/|\Omega| = \sqrt{7}/3$ which is attained at $q = 1/\sqrt{8}$. This value is larger than the Oort A-value $\nu_{\rm A}/|\Omega| = 3/4$.

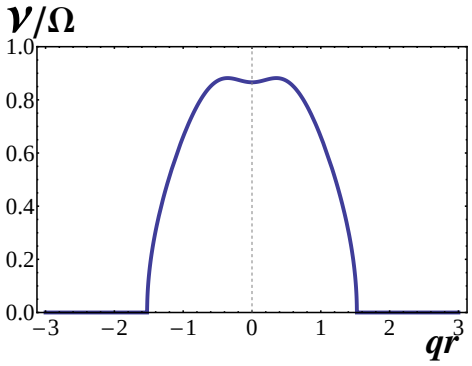

Fig. 9 The growth rate of the non-axisymmetric wave of $m = 1$ and $k \to 0$, versus qr with q being the radial wavenumber, for $Rb = -1$ and $\omega_{A\theta}/\Omega = 1$. The flow is Keplerian ($Ro = -3/4$). The maximum growth rate is $\nu_{max} = \sqrt{7}\Omega/3$ taken at $qr = \pm 1/\sqrt{8}$.

6. Discussions

We have explored the AMRI of a perfectly conducting fluid to non-axisymmetric as well as axisymmetric perturbations of short wavelengths, based on the Hain-Lüst equation (10) augmented with the terms originating from a background flow of differential rotation. The present investigation is capable of dealing with a rotating flow of arbitrary angular velocity profile $\Omega(r)$. The advantage of using the Hain-Lüst equation is that a risk of dropping-off the terms with radial derivatives can be avoided. If we substitute the WKB ansatz $\boldsymbol{\xi} \propto \exp[i \int q(r)\mathrm{d}r]$, at an earlier stage, into (6) say, the derivative in r is replaced by multiplication iq, and after this stage, the operation of radial derivative $iq = \mathrm{d}/\mathrm{d}r$ is liable to be inactive, though it should be. It is safer to keep all the derivative terms to the very last stage where we apply the short wavelength approximation. Retaining all the relevant terms has disclosed rich aspects of the AMRI to non-axisymmetric perturbations than known ones (*cf.* ref [8]).

Given Rb, for small values of $|\omega_{A\theta}/\Omega|$, a rotating flow is unstable to non-axisymmetric perturbations of $|k| \to \infty$ if $Ro < (Rb - 1/4)(\omega_{A\theta}/\Omega)^2$ as dictated by (26), with the maximum growth rate close to the Oort A-value $|Ro|$. For $|\omega_{A\theta}/\Omega| \sim 1$, the situation is changed. When $Rb > -3/4$, the rotating flow is unstable to perturbations of $|k| \to \infty$ in the whole range of Ro. But the mode of $|k| \to \infty$ subsides down as Rb is decreased and disappears at $Rb = -3/4$. Instead, another unstable mode of $k = 0$ emerges at $Rb = -1/4$, develops as Rb is decreased, and surpasses the mode of $|k| \to \infty$ for $Rb \leq -1/\sqrt{8}$. The instability mode of $k = 0$ is confined to a finite range in Ro centered on $Ro = 0$, $Ro^2 < (|Rb| - 1/4)(\omega_{A\theta}/\Omega)^2$ for $-1/2 \leq Rb < -1/4$, and $Ro^2 < Rb^2(\omega_{A\theta}/\Omega)^2$ for $Rb < -1/2$, as is derived from (33).

The behavior, over the whole range of $\omega_{A\theta}/\Omega$, of the modes of $m = 1$ and $|k| \to \infty$ and of $m = 1$ and $k = 0$ is summarized as follows. For $Ro < 0$ and $Rb < -3/4$, the mode of $|k| \to \infty$ is confined approximately to $0 < |\omega_{A\theta}/\Omega| < \sqrt{|Ro|/(|Rb| + 1/4)}$ as is read off from (26). The unstable mode of $k = 0$ exists for $|\omega_{A\theta}/\Omega| > |Ro/Rb|$ when $Ro < -1/2$, and for $|\omega_{A\theta}/\Omega| > |Ro|/\sqrt{|Rb| - 1/4}$ when $-1/2 \leq Ro < -1/4$. The overall behavior for $Ro < 0$ and $Rb < -3/4$ looks like Fig. 8. For $Rb > -3/4$, the mode of $|k| \to \infty$ extends to the entire range of $\omega_{A\theta}/\Omega$, and for $-3/4 < b < -1/\sqrt{8}$, the graph looks like Fig. 7. For $Ro < 0$ and

$Rb > -1/\sqrt{8}$, the mode of $|k| \to \infty$ predominates over the mode of $k = 0$ over the entire range of $\omega_{A\theta}/\Omega$. For $Rb \geq -1/4$, the mode of $k = 0$ disappears. The asymptotic behavior at large values of $|\omega_{A\theta}/\Omega|$ is common for all values of Ro and is given by (31). At small values of $|\omega_{A\theta}/\Omega|$, the mode of $|k| \to \infty$ is confined to $0 < |\omega_{A\theta}/\Omega| < \sqrt{|Ro/(Rb - 1/4)|}$ for $-1/4 < Rb < 1/4$ and $Ro < 0$. This branch is absent for $Ro \geq 0$. For $Rb > 1/4$, this branch exists for $|\omega_{A\theta}/\Omega| > \sqrt{Ro/(Rb - 1/4)}$. As a whole, for $Rb > -1/4$, the graph looks like Fig. 4 for $Ro < 0$ and like Fig. 5 for $Ro > 0$. It is remarkable that the growth rate exceed the Oort A-value by increasing $|\omega_{A\theta}/\Omega|$.

This is not the end of story. We have exclusively explored the unstable modes in the two extremes, $|k| \to \infty$ and $k = 0$, as either of the two is likely to be dominant. However, a detailed examination shows that there are cases that, given Ro and Rb, the mode of the largest growth rate occurs at an intermediate value of k. For instance, given a Keplerian rotation ($Ro = -3/4$), for $|\omega_{A\theta}/\Omega| \ll 1$ and fixing $m = 1$ and $q = 0$, the most unstable mode occurs at an intermediate value of k when $Rb \lesssim -17.5$. Furthermore, the transition of the behavior from $|\omega_{A\theta}/\Omega| \ll 1$ to that of $|\omega_{A\theta}/\Omega| \sim 1$ calls for elaboration.

It is probable that these properties, in particular non-existence of critical Rossby number for large values of Rb, may carry over to the helical MRI (HMRI) for which the both axial and azimuthal magnetic fields are externally imposed. From the practical view point, the inductionless limit is worth pursuing, since the laboratory experiments of using a liquid metal, such as PROMISE (Potsdam ROssendorf Magnetic InStability Experiment) [11], belongs to this regime. As a preliminary study, we have made an attempt to incorporate the viscous and the resistive terms into the Hain-Lüst equation (10). We denote ν_0 and η to be the coefficients of viscosity and electric resistivity, respectively. For $Pm = \nu_0/\eta = 10^{-6}$, $Re = \Omega/(\nu_0 k^2) = 10^5$ and the helical magnetic field of $\beta = B_z k^2/\mu = 1$, the Keplerian rotation is linearly unstable to non-axisymmetric perturbations of $m = 1$, $k = 1$ and $q = 0$. The critical Rossby number for non-axisymmtric case, and in particular the relevance of Liu's limit [16] may well be scrutinized. See also ref [17].

Care is excised for the most unstable mode of $k = 0$ and $q = 0$ which is dominant $|\omega_{A\theta}/\Omega| \sim 1$ for $Rb < -1/\sqrt{8}$. This mode may lie outside the range of validity of the WKB approximation to short-wavelength waves. Moreover, the perturbation of large m invites the action of the viscous and/or resistive cut off. To draw a definite conclusion on the AMRI or HMRI to non-axisymmetric perturbations, the global modal analyses are indispensable. For the purpose of the global stability analyses as well, the Hain-Lüst equation provides us with a sound basis [18]. The determination of the maximum growth rate for the AMRI and the HMRI is left for a future investigation.

Acknowledgements

We are grateful to Oleg N Kirillov for his invaluable guidance for the MRI. R. Z. was supported by PhD Studentship from China Scholarship Council. Y. F. was supported in part by a Grant-in-Aid for Scientific Research from the Japan Society for the Promotion of Science (Grant No. 24540407).

References

[1] E. Velikhov, JETP (USSR) **36**, 1398 (1959).
[2] S. Chandrasekhar, Proc. Natl. Acad. Sci. **46**, 253 (1960).
[3] A. Balbus, and J. F. Hawley, Astrophys. J. **376**, 214 (1991).
[4] S. Chandrasekhar, *Hydrodynamic and Hydromagnetic Stability* (Clarendon Press, Oxford, 1961).

[5] O. N. Kirillov, and F. Stefani, Astrophys. J. **712**, 52 (2010).
[6] O. N. Kirillov, and F. Stefani, Acta Appl. Math. **120**, 177 (2012).
[7] A. Balbus, and J. F. Hawley, Astrophys. J. **392**, 662 (1992).
[8] A. Balbus, and J. F. Hawley, Astrophys. J. **400**, 610 (1992).
[9] S. J. Desch, Astrophys. J. **608**, 509 (2004).
[10] R. Hollerbach, and G. Rüdiger, Phys. Rev. Lett. **95**, 124501 (2005).
[11] F. Stefani, Th. Gundrum, G. Gerbeth, G. Rüdiger, M. Schultz, J. Szklarski, and R. Hollerbach, Phys. Rev. Lett. **97**, 184502 (2006).
[12] G. Rüdiger, M. Gellert, M. Schultz, R. Hollerbach, and F. Stefani, Mon. Not. R. Astron. Soc. **438**, 271 (2014).
[13] J. P. Goedbloed, and S. Poedts, *Principles of Magnetohydrodynamics* (Cambridge University Press. Cambridge, 2004).
[14] J. P. Goedbloed, R. Keppens, and S. Poedts, *Advanced Magnetohydrodynamics* (Cambridge University Press. Cambridge, 2010).
[15] E. Knobloch, Mon. Not. R. Astron. Soc. **255**, 25 (1992).
[16] O. N. Kirillov, F. Stefani, and Y. Fukumoto, Astrophys. J. **712**, 52 (2012).
[17] O. N. Kirillov, F. Stefani, and Y. Fukumoto, Fluid Dyn. Res.,*to appear* (2014).
[18] A. B. Mikhailovskii, J. G. Lominadze, R. M. O. Galvao, A. P. Churikov, N. N. Erokhin, A. I. Smolyakov, and V. S. Tsypin, Phys. Plasmas **15**, 0521038.
[19] R. J. Tayler, Mon. Not. R. Astron. Soc. **161**, 365 (1973).
[20] P. G. Saffman, *Vortex Dynamics* (Cambridge University Press. Cambridge, 1992).
[21] Y. Fukumoto, J. Fluid Mech. **493**, 287 (2003).

List of MI Preprint Series, Kyushu University

The Global COE Program
Math-for-Industry Education & Research Hub

MI

MI2008-1 Takahiro ITO, Shuichi INOKUCHI & Yoshihiro MIZOGUCHI
Abstract collision systems simulated by cellular automata

MI2008-2 Eiji ONODERA
The intial value problem for a third-order dispersive flow into compact almost Hermitian manifolds

MI2008-3 Hiroaki KIDO
On isosceles sets in the 4-dimensional Euclidean space

MI2008-4 Hirofumi NOTSU
Numerical computations of cavity flow problems by a pressure stabilized characteristic-curve finite element scheme

MI2008-5 Yoshiyasu OZEKI
Torsion points of abelian varieties with values in nfinite extensions over a p-adic field

MI2008-6 Yoshiyuki TOMIYAMA
Lifting Galois representations over arbitrary number fields

MI2008-7 Takehiro HIROTSU & Setsuo TANIGUCHI
The random walk model revisited

MI2008-8 Silvia GANDY, Masaaki KANNO, Hirokazu ANAI & Kazuhiro YOKOYAMA
Optimizing a particular real root of a polynomial by a special cylindrical algebraic decomposition

MI2008-9 Kazufumi KIMOTO, Sho MATSUMOTO & Masato WAKAYAMA
Alpha-determinant cyclic modules and Jacobi polynomials

MI2008-10 Sangyeol LEE & Hiroki MASUDA
Jarque-Bera Normality Test for the Driving Lévy Process of a Discretely Observed Univariate SDE

MI2008-11 Hiroyuki CHIHARA & Eiji ONODERA
A third order dispersive flow for closed curves into almost Hermitian manifolds

MI2008-12 Takehiko KINOSHITA, Kouji HASHIMOTO and Mitsuhiro T. NAKAO
On the L^2 a priori error estimates to the finite element solution of elliptic problems with singular adjoint operator

MI2008-13 Jacques FARAUT and Masato WAKAYAMA
Hermitian symmetric spaces of tube type and multivariate Meixner-Pollaczek polynomials

MI2008-14 Takashi NAKAMURA
Riemann zeta-values, Euler polynomials and the best constant of Sobolev inequality

MI2008-15 Takashi NAKAMURA
Some topics related to Hurwitz-Lerch zeta functions

MI2009-1 Yasuhide FUKUMOTO
Global time evolution of viscous vortex rings

MI2009-2 Hidetoshi MATSUI & Sadanori KONISHI
Regularized functional regression modeling for functional response and predictors

MI2009-3 Hidetoshi MATSUI & Sadanori KONISHI
Variable selection for functional regression model via the L_1 regularization

MI2009-4 Shuichi KAWANO & Sadanori KONISHI
Nonlinear logistic discrimination via regularized Gaussian basis expansions

MI2009-5 Toshiro HIRANOUCHI & Yuichiro TAGUCHII
Flat modules and Groebner bases over truncated discrete valuation rings

MI2009-6 Kenji KAJIWARA & Yasuhiro OHTA
Bilinearization and Casorati determinant solutions to non-autonomous 1+1 dimensional discrete soliton equations

MI2009-7 Yoshiyuki KAGEI
Asymptotic behavior of solutions of the compressible Navier-Stokes equation around the plane Couette flow

MI2009-8 Shohei TATEISHI, Hidetoshi MATSUI & Sadanori KONISHI
Nonlinear regression modeling via the lasso-type regularization

MI2009-9 Takeshi TAKAISHI & Masato KIMURA
Phase field model for mode III crack growth in two dimensional elasticity

MI2009-10 Shingo SAITO
Generalisation of Mack's formula for claims reserving with arbitrary exponents for the variance assumption

MI2009-11 Kenji KAJIWARA, Masanobu KANEKO, Atsushi NOBE & Teruhisa TSUDA
Ultradiscretization of a solvable two-dimensional chaotic map associated with the Hesse cubic curve

MI2009-12 Tetsu MASUDA
Hypergeometric τ-functions of the q-Painlevé system of type $E_8^{(1)}$

MI2009-13 Hidenao IWANE, Hitoshi YANAMI, Hirokazu ANAI & Kazuhiro YOKOYAMA
A Practical Implementation of a Symbolic-Numeric Cylindrical Algebraic Decomposition for Quantifier Elimination

MI2009-14 Yasunori MAEKAWA
On Gaussian decay estimates of solutions to some linear elliptic equations and its applications

MI2009-15 Yuya ISHIHARA & Yoshiyuki KAGEI
Large time behavior of the semigroup on L^p spaces associated with the linearized compressible Navier-Stokes equation in a cylindrical domain

MI2009-16 Chikashi ARITA, Atsuo KUNIBA, Kazumitsu SAKAI & Tsuyoshi SAWABE
Spectrum in multi-species asymmetric simple exclusion process on a ring

MI2009-17 Masato WAKAYAMA & Keitaro YAMAMOTO
Non-linear algebraic differential equations satisfied by certain family of elliptic functions

MI2009-18 Me Me NAING & Yasuhide FUKUMOTO
Local Instability of an Elliptical Flow Subjected to a Coriolis Force

MI2009-19 Mitsunori KAYANO & Sadanori KONISHI
Sparse functional principal component analysis via regularized basis expansions and its application

MI2009-20 Shuichi KAWANO & Sadanori KONISHI
Semi-supervised logistic discrimination via regularized Gaussian basis expansions

MI2009-21 Hiroshi YOSHIDA, Yoshihiro MIWA & Masanobu KANEKO
Elliptic curves and Fibonacci numbers arising from Lindenmayer system with symbolic computations

MI2009-22 Eiji ONODERA
A remark on the global existence of a third order dispersive flow into locally Hermitian symmetric spaces

MI2009-23 Stjepan LUGOMER & Yasuhide FUKUMOTO
Generation of ribbons, helicoids and complex scherk surface in laser-matter Interactions

MI2009-24 Yu KAWAKAMI
Recent progress in value distribution of the hyperbolic Gauss map

MI2009-25 Takehiko KINOSHITA & Mitsuhiro T. NAKAO
On very accurate enclosure of the optimal constant in the a priori error estimates for H_0^2-projection

MI2009-26 Manabu YOSHIDA
Ramification of local fields and Fontaine's property (Pm)

MI2009-27 Yu KAWAKAMI
Value distribution of the hyperbolic Gauss maps for flat fronts in hyperbolic three-space

MI2009-28 Masahisa TABATA
Numerical simulation of fluid movement in an hourglass by an energy-stable finite element scheme

MI2009-29 Yoshiyuki KAGEI & Yasunori MAEKAWA
Asymptotic behaviors of solutions to evolution equations in the presence of translation and scaling invariance

MI2009-30 Yoshiyuki KAGEI & Yasunori MAEKAWA
On asymptotic behaviors of solutions to parabolic systems modelling chemotaxis

MI2009-31 Masato WAKAYAMA & Yoshinori YAMASAKI
Hecke's zeros and higher depth determinants

MI2009-32 Olivier PIRONNEAU & Masahisa TABATA
Stability and convergence of a Galerkin-characteristics finite element scheme of lumped mass type

MI2009-33 Chikashi ARITA
Queueing process with excluded-volume effect

MI2009-34 Kenji KAJIWARA, Nobutaka NAKAZONO & Teruhisa TSUDA
Projective reduction of the discrete Painlevé system of type$(A_2 + A_1)^{(1)}$

MI2009-35 Yosuke MIZUYAMA, Takamasa SHINDE, Masahisa TABATA & Daisuke TAGAMI
Finite element computation for scattering problems of micro-hologram using DtN map

MI2009-36 Reiichiro KAWAI & Hiroki MASUDA
Exact simulation of finite variation tempered stable Ornstein-Uhlenbeck processes

MI2009-37 Hiroki MASUDA
On statistical aspects in calibrating a geometric skewed stable asset price model

MI2010-1 Hiroki MASUDA
Approximate self-weighted LAD estimation of discretely observed ergodic Ornstein-Uhlenbeck processes

MI2010-2 Reiichiro KAWAI & Hiroki MASUDA
Infinite variation tempered stable Ornstein-Uhlenbeck processes with discrete observations

MI2010-3 Kei HIROSE, Shuichi KAWANO, Daisuke MIIKE & Sadanori KONISHI
Hyper-parameter selection in Bayesian structural equation models

MI2010-4 Nobuyuki IKEDA & Setsuo TANIGUCHI
The Itô-Nisio theorem, quadratic Wiener functionals, and 1-solitons

MI2010-5 Shohei TATEISHI & Sadanori KONISHI
Nonlinear regression modeling and detecting change point via the relevance vector machine

MI2010-6 Shuichi KAWANO, Toshihiro MISUMI & Sadanori KONISHI
Semi-supervised logistic discrimination via graph-based regularization

MI2010-7 Teruhisa TSUDA
UC hierarchy and monodromy preserving deformation

MI2010-8 Takahiro ITO
Abstract collision systems on groups

MI2010-9 Hiroshi YOSHIDA, Kinji KIMURA, Naoki YOSHIDA, Junko TANAKA & Yoshihiro MIWA
An algebraic approach to underdetermined experiments

MI2010-10 Kei HIROSE & Sadanori KONISHI
Variable selection via the grouped weighted lasso for factor analysis models

MI2010-11 Katsusuke NABESHIMA & Hiroshi YOSHIDA
Derivation of specific conditions with Comprehensive Groebner Systems

MI2010-12 Yoshiyuki KAGEI, Yu NAGAFUCHI & Takeshi SUDOU
Decay estimates on solutions of the linearized compressible Navier-Stokes equation around a Poiseuille type flow

MI2010-13 Reiichiro KAWAI & Hiroki MASUDA
On simulation of tempered stable random variates

MI2010-14 Yoshiyasu OZEKI
Non-existence of certain Galois representations with a uniform tame inertia weight

MI2010-15 Me Me NAING & Yasuhide FUKUMOTO
Local Instability of a Rotating Flow Driven by Precession of Arbitrary Frequency

MI2010-16 Yu KAWAKAMI & Daisuke NAKAJO
The value distribution of the Gauss map of improper affine spheres

MI2010-17 Kazunori YASUTAKE
On the classification of rank 2 almost Fano bundles on projective space

MI2010-18 Toshimitsu TAKAESU
Scaling limits for the system of semi-relativistic particles coupled to a scalar bose field

MI2010-19 Reiichiro KAWAI & Hiroki MASUDA
Local asymptotic normality for normal inverse Gaussian Lévy processes with high-frequency sampling

MI2010-20 Yasuhide FUKUMOTO, Makoto HIROTA & Youichi MIE
Lagrangian approach to weakly nonlinear stability of an elliptical flow

MI2010-21 Hiroki MASUDA
Approximate quadratic estimating function for discretely observed Lévy driven SDEs with application to a noise normality test

MI2010-22 Toshimitsu TAKAESU
A Generalized Scaling Limit and its Application to the Semi-Relativistic Particles System Coupled to a Bose Field with Removing Ultraviolet Cutoffs

MI2010-23 Takahiro ITO, Mitsuhiko FUJIO, Shuichi INOKUCHI & Yoshihiro MIZOGUCHI
Composition, union and division of cellular automata on groups

MI2010-24 Toshimitsu TAKAESU
A Hardy's Uncertainty Principle Lemma in Weak Commutation Relations of Heisenberg-Lie Algebra

MI2010-25 Toshimitsu TAKAESU
On the Essential Self-Adjointness of Anti-Commutative Operators

MI2010-26 Reiichiro KAWAI & Hiroki MASUDA
On the local asymptotic behavior of the likelihood function for Meixner Lévy processes under high-frequency sampling

MI2010-27 Chikashi ARITA & Daichi YANAGISAWA
Exclusive Queueing Process with Discrete Time

MI2010-28 Jun-ichi INOGUCHI, Kenji KAJIWARA, Nozomu MATSUURA & Yasuhiro OHTA
Motion and Bäcklund transformations of discrete plane curves

MI2010-29 Takanori YASUDA, Masaya YASUDA, Takeshi SHIMOYAMA & Jun KOGURE
On the Number of the Pairing-friendly Curves

MI2010-30 Chikashi ARITA & Kohei MOTEGI
Spin-spin correlation functions of the q-VBS state of an integer spin model

MI2010-31 Shohei TATEISHI & Sadanori KONISHI
Nonlinear regression modeling and spike detection via Gaussian basis expansions

MI2010-32 Nobutaka NAKAZONO
Hypergeometric τ functions of the q-Painlevé systems of type $(A_2 + A_1)^{(1)}$

MI2010-33 Yoshiyuki KAGEI
Global existence of solutions to the compressible Navier-Stokes equation around parallel flows

MI2010-34 Nobushige KUROKAWA, Masato WAKAYAMA & Yoshinori YAMASAKI
Milnor-Selberg zeta functions and zeta regularizations

MI2010-35 Kissani PERERA & Yoshihiro MIZOGUCHI
Laplacian energy of directed graphs and minimizing maximum outdegree algorithms

MI2010-36 Takanori YASUDA
CAP representations of inner forms of $Sp(4)$ with respect to Klingen parabolic subgroup

MI2010-37 Chikashi ARITA & Andreas SCHADSCHNEIDER
Dynamical analysis of the exclusive queueing process

MI2011-1 Yasuhide FUKUMOTO& Alexander B. SAMOKHIN
Singular electromagnetic modes in an anisotropic medium

MI2011-2 Hiroki KONDO, Shingo SAITO & Setsuo TANIGUCHI
Asymptotic tail dependence of the normal copula

MI2011-3 Takehiro HIROTSU, Hiroki KONDO, Shingo SAITO, Takuya SATO, Tatsushi TANAKA & Setsuo TANIGUCHI
Anderson-Darling test and the Malliavin calculus

MI2011-4 Hiroshi INOUE, Shohei TATEISHI & Sadanori KONISHI
Nonlinear regression modeling via Compressed Sensing

MI2011-5 Hiroshi INOUE
Implications in Compressed Sensing and the Restricted Isometry Property

MI2011-6 Daeju KIM & Sadanori KONISHI
Predictive information criterion for nonlinear regression model based on basis expansion methods

MI2011-7 Shohei TATEISHI, Chiaki KINJYO & Sadanori KONISHI
Group variable selection via relevance vector machine

MI2011-8 Jan BREZINA & Yoshiyuki KAGEI
Decay properties of solutions to the linearized compressible Navier-Stokes equation around time-periodic parallel flow
Group variable selection via relevance vector machine

MI2011-9 Chikashi ARITA, Arvind AYYER, Kirone MALLICK & Sylvain PROLHAC
Recursive structures in the multispecies TASEP

MI2011-10 Kazunori YASUTAKE
On projective space bundle with nef normalized tautological line bundle

MI2011-11 Hisashi ANDO, Mike HAY, Kenji KAJIWARA & Tetsu MASUDA
An explicit formula for the discrete power function associated with circle patterns of Schramm type

MI2011-12 Yoshiyuki KAGEI
Asymptotic behavior of solutions to the compressible Navier-Stokes equation around a parallel flow

MI2011-13 Vladimír CHALUPECKÝ & Adrian MUNTEAN
Semi-discrete finite difference multiscale scheme for a concrete corrosion model: approximation estimates and convergence

MI2011-14 Jun-ichi INOGUCHI, Kenji KAJIWARA, Nozomu MATSUURA & Yasuhiro OHTA
Explicit solutions to the semi-discrete modified KdV equation and motion of discrete plane curves

MI2011-15 Hiroshi INOUE
A generalization of restricted isometry property and applications to compressed sensing

MI2011-16 Yu KAWAKAMI
A ramification theorem for the ratio of canonical forms of flat surfaces in hyperbolic three-space

MI2011-17 Naoyuki KAMIYAMA
Matroid intersection with priority constraints

MI2012-1 Kazufumi KIMOTO & Masato WAKAYAMA
Spectrum of non-commutative harmonic oscillators and residual modular forms

MI2012-2 Hiroki MASUDA
Mighty convergence of the Gaussian quasi-likelihood random fields for ergodic Levy driven SDE observed at high frequency

MI2012-3 Hiroshi INOUE
A Weak RIP of theory of compressed sensing and LASSO

MI2012-4 Yasuhide FUKUMOTO & Youich MIE
Hamiltonian bifurcation theory for a rotating flow subject to elliptic straining field

MI2012-5 Yu KAWAKAMI
On the maximal number of exceptional values of Gauss maps for various classes of surfaces

MI2012-6 Marcio GAMEIRO, Yasuaki HIRAOKA, Shunsuke IZUMI, Miroslav KRAMAR, Konstantin MISCHAIKOW & Vidit NANDA
Topological Measurement of Protein Compressibility via Persistence Diagrams

MI2012-7 Nobutaka NAKAZONO & Seiji NISHIOKA
Solutions to a q-analog of Painlevé III equation of type $D_7^{(1)}$

MI2012-8 Naoyuki KAMIYAMA
A new approach to the Pareto stable matching problem

MI2012-9 Jan BREZINA & Yoshiyuki KAGEI
Spectral properties of the linearized compressible Navier-Stokes equation around time-periodic parallel flow

MI2012-10 Jan BREZINA
Asymptotic behavior of solutions to the compressible Navier-Stokes equation around a time-periodic parallel flow

MI2012-11 Daeju KIM, Shuichi KAWANO & Yoshiyuki NINOMIYA
Adaptive basis expansion via the extended fused lasso

MI2012-12 Masato WAKAYAMA
On simplicity of the lowest eigenvalue of non-commutative harmonic oscillators

MI2012-13 Masatoshi OKITA
On the convergence rates for the compressible
Navier- Stokes equations with potential force

MI2013-1 Abuduwaili PAERHATI & Yasuhide FUKUMOTO
A Counter-example to Thomson-Tait-Chetayev's Theorem

MI2013-2 Yasuhide FUKUMOTO & Hirofumi SAKUMA
A unified view of topological invariants of barotropic and baroclinic fluids and their application to formal stability analysis of three-dimensional ideal gas flows

MI2013-3 Hiroki MASUDA
Asymptotics for functionals of self-normalized residuals of discretely observed stochastic processes

MI2013-4 Naoyuki KAMIYAMA
On Counting Output Patterns of Logic Circuits

MI2013-5 Hiroshi INOUE
RIPless Theory for Compressed Sensing

MI2013-6 Hiroshi INOUE
Improved bounds on Restricted isometry for compressed sensing

MI2013-7 Hidetoshi MATSUI
Variable and boundary selection for functional data via multiclass logistic regression modeling

MI2013-8 Hidetoshi MATSUI
Variable selection for varying coefficient models with the sparse regularization

MI2013-9 Naoyuki KAMIYAMA
Packing Arborescences in Acyclic Temporal Networks

MI2013-10 Masato WAKAYAMA
Equivalence between the eigenvalue problem of non-commutative harmonic oscillators and existence of holomorphic solutions of Heun's differential equations, eigenstates degeneration, and Rabi's model

MI2013-11 Masatoshi OKITA
Optimal decay rate for strong solutions in critical spaces to the compressible Navier-Stokes equations

MI2013-12 Shuichi KAWANO, Ibuki HOSHINA, Kazuki MATSUDA & Sadanori KONISHI
Predictive model selection criteria for Bayesian lasso

MI2013-13 Hayato CHIBA
The First Painleve Equation on the Weighted Projective Space

MI2013-14 Hidetoshi MATSUI
Variable selection for functional linear models with functional predictors and a functional response

MI2013-15 Naoyuki KAMIYAMA
The Fault-Tolerant Facility Location Problem with Submodular Penalties

MI2013-16 Hidetoshi MATSUI
Selection of classification boundaries using the logistic regression

MI2014-1 Naoyuki KAMIYAMA
Popular Matchings under Matroid Constraints

MI2014-2 Yasuhide FUKUMOTO & Youichi MIE
Lagrangian approach to weakly nonlinear interaction of Kelvin waves and a symmetry-breaking bifurcation of a rotating flow

MI2014-3 Reika AOYAMA
Decay estimates on solutions of the linearized compressible Navier-Stokes equation around a Parallel flow in a cylindrical domain

MI2014-4 Naoyuki KAMIYAMA
The Popular Condensation Problem under Matroid Constraints

MI2014-5 Yoshiyuki KAGEI & Kazuyuki TSUDA
Existence and stability of time periodic solution to the compressible Navier-Stokes equation for time periodic external force with symmetry

MI2014-6 This paper was withdrawn by the authors.

MI2014-7 Masatoshi OKITA
On decay estimate of strong solutions in critical spaces for the compressible Navier-Stokes equations

MI2014-8 Rong ZOU & Yasuhide FUKUMOTO
Local stability analysis of azimuthal magnetorotational instability of ideal MHD flows